Silent Death by Sound: C_{60} Fullerene Sonodynamic Treatment of Cancer Cells

Aleksandar Radivoievych
Technical University of Applied Sciences Wildau
Benjamin Kolp
Technical University of Applied Sciences Wildau
Sergii Grebinyk
Technical University of Applied Sciences Wildau
Svitlana Prylutska
Taras Shevchenko National University of Kyiv
Uwe Ritter
Ilmenau University of Technology
Oliver Zolk
Medizinische Hochschule Brandenburg Theodor Fontane
Jörn Glökler
Technical University of Applied Sciences Wildau
Marcus Frohme (mfrohme@th-wildau.de)
Technical University of Applied Sciences Wildau
Anna Grebinyk
Technical University of Applied Sciences Wildau

Research Article

Keywords: Ultrasound, C60 fullerene, sonodynamic therapy, HeLa cells, apoptosis

Posted Date: January 3rd, 2022

DOI: https://doi.org/10.21203/rs.3.rs-1193610/v1

Abstract

The acoustic pressure waves of ultrasound (US) penetrate biological tissues deeper than light. Another important feature of US its potential to generate light emission within the excited medium termed sonoluminescence. This promoted the idea of its use as an alternative energy source for photosensitizer excitation. Pristine C_{60} fullerene (C_{60}), an excellent photosensitizer, was explored in the frame of cancer sonodynamic therapy (SDT). For that purpose, we analyzed C_{60} effects on human cervix carcinoma HeLa cells in combination with a low intensity US treatment.

The time-dependent accumulation of C_{60} in HeLa cells reached its maximum at 24 h (800 ± 66 ng / 10^6 cells). Half of extranuclear C_{60} localized within mitochondria. The efficiency of C_{60} nanostructure's sonoexcitation with 1 MHz US was tested with cell viability assay. A significant proapoptotic sonotoxic effect was found for HeLa cells.

C_{60}'s ability to induce apoptosis of carcinoma cells after sonoexcitation with US provides a promising novel approach for cancer treatment.

Background

Closed-sphere carbon nanostructure C60 fullerene [1] (here consistently abbreviated "C60") is used for several biomedical applications since its unique structure can elicit antiviral, antimicrobic and anticancer activities [2]. The specific packing of sixty carbon atoms in penta- and hexagon units arranges a rather unusual $sp^{2,3}$ hybridization structure [3] with a surface three times smaller than expected for a respective molecular weight. Given carbon bonds similar to the planar graphene, C60's non-planar π-conjugated system of molecular orbitals determines its significant absorption of UV-vis light. After light absorbance a photoexcited C60 molecule can generate reactive oxygen species (ROS) through energy or electron transfer to oxygen [4]. The low photobleaching, high quantum yield and photostability [5] of C60 molecule boosted the rapid development of its application in cancer therapy as a photosensitizer [2, 4, 5, 6]. Previously, negligible toxicity of pristine C_{60} stable colloid solution [7] against normal cells was shown [8, 9]. At the same time a pronounced ROS-mediated proapoptotic effect through a mitochondrial pathway was detected in cancer cells treated with pristine C60 and irradiated with visible light [10, 11, 12]. The further development of C60 as a photosensitizer in the frame of cancer photodynamic therapy (PDT) is hampered by its relatively high band gap [13] and, therefore, low absorbance of the tissue penetrating long-wavelength [14] light. Moreover, PDT faces the heterogeneous nature of biological tissues that can affect the original path of photons due to the high absorption, scattering and anisotropy [15].

The deep penetration of ultrasound (US) waves in biological tissues beyond the reach of external light has promoted the idea of using them as an alternative energy source for the excitation of photosensitizers. The sonodynamic therapy (SDT), derived from the PDT, recently emerged as a non-invasive cancer treatment modality relying on the activation of certain chemical sensitizers with US. It has been generally accepted that the cavitation effect of US is responsible for the SDT mechanism [16].

Acoustic cavitation is a unique physical phenomenon involving the formation, growth and collapse of bubbles during the propagation of US waves in liquids. The explosion of bubbles leads to a sonoluminescence, that releases the accumulated energy [17]. The sonoluminescence spectrum in water is relatively broadband with an UV maximum and a long-wavelength tail [18, 19, 20]. It has been shown that the cavitation bubbles generated by ultrasound not only transform sound into light, but also cause pyrolysis and increase the temperature, that can be attributed to the modulation of toxic effects as well [21]. Various organic sonosensitizers have been adopted from PDT to SDT, including aminolevulinic acid [22, 23], Rose Bengal [24] and porphyrins [25]. Compared to organic sonosensitizers, inorganic nanoparticles such as gold [26], silicon [27] and titanium dioxide [28] offer relatively high chemical and physiological stability and have also been demonstrated to be effective in SDT. The polyethylene glycol- [29], polyhydroxy [30] and tris-acid [31] fullerenes have been also shown to efficiently induce ROS-mediated compact apoptotic cancer cell death once used in SDT. The pristine C_{60}'s higher lipophilicity over its derivatives promotes its faster diffusion across the plasma membrane and facilitates intracellular uptake [32, 33]. Owing to the nature of sonoluminiscence and its spectrum in particular [18, 19, 20], US seems to be a good matching option for activating pristine C_{60} to generate ROS.

Herein, we report the first data to our knowledge on the use of 1 MHz US application for sonosexcitation of pristine C60 to treat carcinoma cells, examining the intracellular accumulation of C60 and the mechanism of cell death.

Results

C_{60} aqueous colloid solution

To determine the most abundant molecular ions in the aqueous C60 solution used, the MALDI-TOF-MS (matrix assisted laser desorption ionization-time of flight mass spectrometry) method was employed. This method can be used to ensure that the preparation of C60 in water has not caused any changes to the fullerene structure. The MALDI-TOF-MS analysis of C60 samples revealed sharply defined peaks for a predominant molecular mass of 720 Da (Fig. 1a). The obtained spectrum confirms the presence of naturally occurring stable isotopes of common element carbon resulted in the gradual triplication of the peak. Only 98.89% of naturally occurring carbon atoms are in the form of 12C; most of the remaining 1.11% consists of atoms of 13C and trace amount of 14C [34]. The presence of one 13C atom in C60 molecule shifted mass to 721 Da and 722 Da molecule had two 13C atoms in the cage, respectively.

In order to check the stability of aqueous colloid solution the size distribution was monitored with dynamic light scattering. The average of C_{60} nanoparticles was evaluated to be 120 nm (Fig. 1b) that matched previous investigations [7, 35] and evidenced storage stability during 6 months.

Sonoluminescence detection

To prove existence of the sonoluminescence, the optical measurements were done with a sensitive photomultiplier tube, able to detect even a single photon via photoelectric effect and secondary emission. Obtained Vpp (peak-to-peak voltage) data on light intensity were recorded in US bath during 100-500 W output power of US generator and normalized with the respective Vpp obtained when the shutter of the photomultiplier window was closed with the US on. The detected increase of the Vpp proved the existence of the sonoluminescence during 1 MHz US propagation through degassed distilled water in the water bath (Fig. 2). In addition, the level of the detected sonoluminescence was increased with the higher output power of the US generator. Thus, the increase of the output power of the US generator from 100 to 500 W resulted in a 44% increase in the detected Vpp signal. Next, the sonoluminescence level in water the bath with a well plate was investigated to mimic conditions, required for cell-based assays. The obtained Vpp from the photomultiplier tube evidenced the decrease of the sonoluminescence level in the well plate as compared to the sonoluminescence level in the bath. However, the Student's test confirmed its dose-dependent significant positive correlation with the output power of US generator as well. Therefore, it can be concluded that sonoluminescence occurred during 1 MHz US propagation in the experimental set-up, required for cell-based assays.

Intracellular C_{60} accumulation

The intracellular uptake and distribution of C60 was studied by fluorescence immunostaining of HeLa cells using a FITC-labeled sandwich of antibodies against C60. Figure 3a presents the images of HeLa cells stained after incubation with 20 μM C60 for 24 h. Simultaneously, cells were stained with DNA-binding dye DAPI for cell nucleus and membrane-potential-sensitive MitoTracker Orange for mitochondria visualization. The detected green fluorescence evidenced C60 uptake and clear extranuclear localization.

To study the accumulation dynamics, we have extracted C60 from the cell homogenate as well as from the mitochondrial fraction and carried out HPLC-ESI-MS (high-performance liquid chromatography/electrospray ionization tandem mass spectrometry) analysis. The observed time-dependent intracellular uptake of C60 reached a maximum of 800 ± 66 ng/10^6 cells after 24 h of incubation (Fig. 3b). The intracellular amount of C_{60} in the HeLa cells was found to be 3 times higher as compared with human leukemic CCRF-CEM cells, as investigated before [10, 36], potentially a result of the much higher cytosol/nucleus volume ratio.

The next step was to quantify C60 content in the mitochondria using both fluorescence image processing and HPLC-ESI-MS. C60 content in the mitochondria fraction showed accumulation at a level of < 380 ± 30 ng/10^6 cells at 24 h, representing 47% of its overall cellular content. The yellow color in the merged fluorescence images verified a partial co-localization of green C_{60} antibodies and red mitochondrial marker. Our data demonstrated a high accumulation of C60 within mitochondria of HeLa cells.

Cell viability

To assess whether sonodynamic treatment of HeLa cells incubated with C_{60} could have any toxic effects, cell viability was analyzed. Cells were treated with 20 μM C_{60} for 24 h, exposed to 1 MHz US and after further 48 h their viability was estimated by MTT (3-(4,5-dimethylthiazol-2-yl)-2,5-diphenyl tetrazolium bromide) assay. The described conditions were selected after “try-and-fail” rigorous comparisons of the US treatment’s effects on the temperature of the liquids in well-plates as well as on cell viability (data not shown). It was found that the US intensity of 5.4 W/cm^2 could be safely used for the treatment mode up to 60 sec, keeping the temperature under 38°C without any significant changes in viability of the cells. The “solvent” control cells incubated with the equal volume of sterile water and treated with US were found to exhibit no significant HeLa cell viability changes that excluded a possible effect of the medium dilution and hypotonicity with addition of aqueous C_{60} solution on the US treatment of cells. The viability of the respective control cells with neither C_{60} nor US treatment was considered as 100%. Without US treatment, no effect was recognizable in the C_{60}-containing control as cell viability remained on the level of 93-96 ± 3-4%. However, the application of US in the presence of C_{60} led to the gradual decrease of the cells’ viability. The US dose of 60 sec in the presence of 20 μM C_{60} decreased the cell viability to 59 ± 5% (Fig. 4a). Visual changes in cell quantity and morphology were also observed with the phase-contrast microscopy. As shown on Figure 4b, HeLa cells, exposed to combined treatment of 1 MHz US and 20 μM C_{60}, demonstrated a decrease of viable cells. Our results evidenced that 1 MHz US induced significant cytotoxic effects of C_{60} against human carcinoma cells.

Apoptosis induction

Cytotoxic effects of photoexcited C_{60} are considered to induce the mitochondrial apoptotic pathway of cell death [4, 12]. However, a similar sonosensitizing toxicity of intracellular accumulated C60 inducing apoptosis had to be proven. Thus, our final goal was to evaluate caspase 3/7 activity and plasma membrane phosphatidylserine translocation evidencing for apoptosis.

No significant effect of either C60 or 1 MHz US alone on caspase 3/7 activity of HeLa cells was observed following 3 h of cells incubation. However, treatment of cells with C60 and US was followed by increase of caspase 3/7 activity. Thus, caspase 3/7 activity was increased to 128 ± 13, 162 ± 16 and 342 ± 29% in HeLa cells, incubated with 20 μM C60 for 24 h and subjected to 1 MHz US treatment for 20, 40 and 60 sec, correspondingly (Fig. 5a).

HeLa cells, treated with C_{60} and US, were subjected to double staining with phosphatidylserine-binding Annexin V-FITC and DNA-binding dye propidium iodide (Fig. 5b). The control cells had a viability of 88 ± 4%. Neither treatment with 20 μM C60 nor US alone had significant effect on cell distribution profiles in FACS (fluorescence-activated cell sorting), demonstrating a viability rate of 83-87 ± 3%. However, under combined action of C60 and 1 MHz US a significant increase in the content of apoptotic HeLa cells was detected, that reached the level of 83 ± 4%, compared to 11 ± 1% of control cells, treated with C60 and kept in the dark (Fig. 5b,c).

Discussion

The common trend in recent years to investigate C_{60} has shown its prospective to mediate PDT of diverse diseases. Most of these reports have been limited to *in vitro* studies where not only cancer cells but also viruses, bacteria, fungi [4, 5] have been incubated with functionalized or solubilized C_{60} followed by light illumination. Light sources usually provided UV, blue, green or white because of the high C_{60} absorption in lower wavelengths with three intense bands in the UV region and a broad tail up to the red light [7, 10]. Since *in vivo* PDT commonly uses red light for its tissue-penetrating properties, it was unclear whether C_{60} would mediate effective PDT *in vivo*. However, such concerns were addressed in a study of intraperitoneal photodynamic C_{60} therapy on a mouse model of abdominal dissemination of colon adenocarcinoma [37]. The synthesis of new C_{60} derivatives and nanocomplexes presents alternative possibility to advance C_{60}-based PDT [38, 39].

Alternatively, rather than altering the photosensitizer molecule, research can also be focused on other sources of its excitation. Thus, a deeper penetration of US waves into biological tissues provides an intriguing opportunity to use them an alternative energy source for sensitizer excitation [16]. The present study evaluates perspectives of US in combination with pristine C_{60} as a sonosensitizer using a stable colloid pristine form for the treatment of carcinoma cells. US is used to deliver mechanical energy with its acoustic pressure wave in a non-invasive manner with minimal thermal effects due to its low intensity. Cavitation that occurs during acoustic pressure wave propagation through the liquid causes gas bubbles to implode with short bursts of light, known as a sonoluminescence. Obtained results confirm the generation of sonoluminescence in the US bath and in the well of the plate exposed to ultrasound irradiation. Intensity of sonoluminescence increased with the output power of US generator. Sonoluminescence spectrum [40] overlaps with the absorbance spectrum of C_{60}, suggesting that it could induce cytotoxic photosensitizing activity of C_{60} [10, 41].

As C_{60} is a hydrophobic molecule able to penetrate lipid bilayers [42] it can translocate through the cell plasma membrane [33, 43]. A low own fluorescence intensity challenged the direct investigation of C_{60} intracellular accumulation with simple and reliable fluorescence-based techniques. The development of a monoclonal antibody against C_{60} conjugated to bovine serum albumin [44, 45] made the indirect immunostaining of pristine C_{60} molecule possible. Recently we optimized this for human leukemic CCRF-CEM cells [10], however, this technique could not be used to evaluate C_{60}'s intracellular concentration and accumulation dynamics. In that case, the optimal solution would be using liquid chromatography mass-spectrometry analysis, that allows a definitive identification and reproducible quantification of trace-level analytes in complex samples. This method was previously reported to be an effective tool for C_{60} quantification in water samples [46] and CCRF-CEM cells [10]. The combination of those methods enabled visualization and quantification of the intracellular accumulation of pristine C_{60} in HeLa cells.

HeLa cells were shown to take up pristine C_{60} from the media in a time-dependent manner. The maximum of intracellular C_{60} level reached 802 ± 66 ng / 10^6 cells after 24 h of incubation (Fig. 3b). The co-staining

with nuclear and mitochondrial markers pointed towards a mitochondrial localization, which was further confirmed with differential centrifugation and HPLC-ESI-MS analysis. C_{60} exhibited predominant localization within mitochondria with 47 % of its overall content in cell extract (Fig. 3a). The mitochondrial localization could be linked with C_{60}'s high electronegativity and a resulting affinity to the mitochondria-associated proton pool [33, 47]. According to density functional theory simulations, C_{60}diffuses into the protonated mitochondrial intermembrane space, where it interacts with up to 6 protons, acquiring a positive charge (Chistyakov et al. 2014). A recent study [48] revealed that the antioxidant protective effect on *Escherichia coli* stems from C_{60}-mediated proton transfer and intracellular interaction with free radicals. Hypothetically C_{60}'s properties as a mitochondria-targeted agent [48] are based on similar mechanisms. This phenomenon is common to carboxyfullerenes [49] and other negatively charged carbon nanoparticles such as single walled carbon nanotubes [50].

For investigation of the combined effect of C_{60} and US, HeLa cells were incubated in the absence or presence of 20 µM C_{60} for 24 h and exposed to 1 MHz US at the spatial average, temporal average intensity I_{SATA} in 5.4 W/cm^2 for different exposure times (≤ 60 sec). After another 48 h of incubation their viability gradually decreased to 59 ± 5 % (Fig. 4), caspase 3/7 activity was induced (Fig. 5a) and cell death differentiation analysis distinguished apoptosis in early and late stages under action of sonodynamically excited C_{60} (Fig. 5b,c).

Our results suggest the potential application of US in combination with pristine C_{60} for sonodynamic treatment of cancer cells. Caspase 3/7 activity was most strongly increased during 60 sec US treatment in the presence of C_{60} as compared to other durations (Fig. 5a), indicating a dose-dependent apoptosis induction during combined cellular treatment with C_{60} and 1 MHz US. In the current study, the specific 1 MHz US treatment set-up was developed to study cellular effects on HeLa cells in the combination with the excellent photosensitizer C_{60} [4, 5, 6, 10]. In order to follow up on previous studies that have evidenced sonodynamic effects of the C_{60} derivatives towards cells *in vitro* [29, 30, 31], the US set-up for treatment of cells was designed as a submersed model corresponding to a “well on water surface” configuration [51]. Constant monitoring of the possible US effects on the temperature of the liquids in well-plates as well as on the cell viability (including “solvent” controls with sterile water equal to the volume for C_{60}) could confirm that the observed biological response can be attributed to the toxic effect of the combined treatment of cells with C_{60} and US. Further optimization of the US treatment of cells and tests with a “sealed well” configuration [51, 52] are planned to prevent any possible undesired US parameter variations in order to apply the combined treatment strategy with C_{60} and 1 MHz US to additional cancer models on cellular, tissue and animal levels. The exact mechanisms underlying the C_{60} sonoexcitation and apoptosis induction during SDT are yet unknown. For therapeutic application, any possible side-effect of US on the body homeostasis should be excluded. However, the typical diagnostic imaging employs US in a very similar frequency range and is known to be safe [53]. As the WHO considers spatial and temporal average intensity I_{SATA} of US ≤3 W/cm^2 as a safe limit for therapeutic ultrasound treatment

[54], it may well be possible to adapt our present experimental model to a real therapeutic setting for treating diseases such as cancer.

Methods

Chemicals

Dulbecco's modified Eagle's medium (DMEM), phosphate-buffered saline (PBS), fetal bovine serum (FBS), penicillin/streptomycin, l-glutamin, and Trypsin were obtained from Biochrom (Berlin, Germany). Poly-D-lysine hydrobromide, Triton X100, Bovine Serum Albumin, p-phenylenediamine, glycerol and 3-(4,5-dimethylthiazol-2-yl)-2,5-diphenyl tetrazolium bromide (MTT) were obtained from Sigma-Aldrich Co. (St-Louis, MO, USA). Paraformaldehyde, toluene, 2-isopropanol, methanol and acetonitrile (both HPLC-MS grade), tris(hydroxymethyl)aminomethane and ethylene glycol-bis(β-aminoethyl ether)-N,N,N',N'-tetraacetic acid, dimethylsulfoxide (DMSO) and trypan blue were used from Carl Roth GmbH + Co. KG (Karlsruhe, Germany).

C_{60} synthesis

The pristine C_{60} aqueous colloid solution was prepared by C_{60} transfer from toluene to water using continuous ultrasound sonication as described by Ritter et al. [7]. The obtained aqueous colloid solution of C_{60} was characterized by 0.2 mM C_{60} concentration, 99 % purity, stability, and homogeneity [7, 35].

Matrix assisted laser desorption ionization-time of flight mass spectrometry

An AximaConfidence Matrix Assisted Laser Desorption Ionization-Time of Flight Mass Spectrometry (MALDI-TOF-MS, Shimadzu, Kyoto, Japan) was used to determine the mass of molecular species in C_{60} colloid solution. Sample (1 µL) was mixed with equal volume of saturated matrix solution (6.5 mM 2,5-dihidrobenzoic acid in 0.1 % trifluoroacetic acid, 50 % acetonitrile) and spotted on a stainless steel target plate and dried. Desorption and ionization were achieved using a 337 nm nitrogen laser. Mass spectra were obtained at maximal laser repetition rate of 50 Hz within a mass range from 0 to 3000 Da. The MALDI-TOFmass spectrometer was calibrated externally using a mixture of standard peptides: Bradykinin fragment 1-7 (757.40 Da), Angiotensin II (human, 1046.54 Da), $P_{14}R$ (synthetic peptide, 1533.86 Da) and ACTH fragment 18-39 (human, 2465.20 Da) from ProteoMass Peptide&Protein MALDI-MS Calibration Kit. To generate representative profiles, a total of 600 laser shots were accumulated and averaged for each sample. MALDI-TOF-MS data processing was performed using the LaunchpadTM v.2.9 Software (Shimadzu, Kyoto, Japan).

Dynamic light scattering

Short ultrasonication (30 sec, 35 kHz) was applied to remove air bubbles. Size distribution of C_{60} aqueous colloid solution was evaluated with a Zetasizer Nano S equipped with a He-Ne 633 nm laser (Malvern Instruments, UK). Data were recorded at 37 °C in backscattering mode at a scattering angle of 173°. C_{60}, placed in disposable polystyrene cuvettes, was measured 15 times to establish average diameters and intensity distributions. The autocorrelation function of the scattered light intensity was analyzed by the Malvern Zetasizer Software (Malvern Instruments, UK) with the Smoluchowski approximation.

Ultrasound exposure set-up

The water for the ultrasound water bath was previously degassed with the vacuum pump Savant UVS 400A SpeedVac (Thermo Fisher Scientific Inc., Berlin, Germany). For precise positioning of the plates inside the US water bath, especially the distance between transducer and plate, a plate holder was designed in SOLIDWorks (Dassault Systems, Massachusetts, USA) and 3D printed by ViNN:Lab (Technical University of Applied Sciences Wildau, Germany). The position of the plate holder was aligned precisely with the US transducer and marked for identical positioning of the well plate during every experiment. The well plate in that way was positioned in 25 mm from the US transducer. Plates with cells, seeded and treated with C_{60} according to the type of the assay described below, were prepared for US treatment. To hinder overheating of the plate, every empty well as well as the spaces between the wells on the plate were filled with 100 µL of filtered water. The US treatment was performed with the US generator 68101 coupled with an MH2 transducer, which was mounted on a water bath (Kaijo, Tokyo, Japan). The US transducer itself was a stainless steel transducer plate installed into a polypropylene tank filled with degassed water. The US transducer had an area of 136x81 mm and a frequency in 950 kHz (~ 1 MHz). The apparatus for the US exposure is shown schematically in Figure 6. The US transducer was driven at 500 W in continuous mode, that correlated to the spatial average, temporal average intensity I_{SATA} of US in 5.4 W/cm^2. The temperature of the sample solution was monitored with a digital thermometer. Thus, different locations of a well as well as a space between wells were compared during different US treatment duration. No temperature increase was found for well plate filled with cell culture medium, preincubated at 37 °C and subjected to the US treatment for 60 sec at 500 W, which longer treatment duration a temperature increase was detected, therefore, the ultrasound treatment duration was limited to 60 sec.

Sonoluminescence detection

The experimental setup for sonoluminescence detection consisted of the photomultiplier tube Hamamatsu R928 (Hamamatsu Photonics, Japan), connected with the Oscilloscope Voltcraft 6150c (Conrad Electronic, Germany) and the power supply Thorn EMI PM28B (Thorn Lighting Ltd, United

Kingdom). The 24-well plate was used because its wells match the diameter of the photomultiplier window. US bath and plate were filled with degassed distilled water for better sonication and sonoluminescence intensity [55]. A polyfoam holder was used to position the photomultiplier on top of a well of the 24-well plate. The US bath was additionally coated with aluminum foil and measurements were performed in a dark room to shield the photomultiplier tube from any external light. The photomultiplier tube was used to detect light from sonoluminescence. The obtained data are presented in voltage. A peak-to-peak voltage for the entire waveform (Vpp) during 120 sec was chosen as an indicator of sonoluminescence as an index of a full voltage between positive and negative peaks of the detected waveform of voltage from the photomultiplier.

Cell culture

The human cervix adenocarcinoma cell line HeLa (ACC 57) was kindly provided by Dr. Müller (Division of Gastroenterology, Infectiology and Rheumatology, Charité – Universitätsmedizin Berlin, Germany).

Cells were maintained in DMEM, supplemented with 10 % FBS, 1 % penicillin/streptomycin and 2 mM glutamine and cultured in 25 cm^2 flasks at 37 °C with 5 % CO_2 in a humidified incubator binder (Tuttlingen, Germany). Treatment with Trypsin (1:10 in PBS) was used to detach adherent cells. The number of viable cells was counted upon 0.1 % trypan blue staining with a Roche Cedex XS analyzer (Basel, Switzerland).

Visualization of intracellular C_{60} accumulation

HeLa cells (10^5/mL) were seeded in 6-well plates on glass coverslips, previously coated with poly-D-Lysine, and incubated for 24 h. Cells were treated with 20 μM C_{60} colloid solution for further 24 h. C_{60} molecules inside cells were visualized with immunofluorescence staining and fluorescence microscopy. Specific fluorescent dyes were used for co-visualization of subcellular compartments such as mitochondria and nuclei – MitoTracker Orange FM (Invitrogen Molecular Probes, Carlsbad, USA) and 4',6-diamidine-2'-phenylindole dihydrochloride (DAPI, Sigma-Aldrich Co., St-Louis, USA), respectively. For staining of the mitochondria, cells were washed with PBS and stained with the MitoTracker Orange FM for 30 min at 37^0C. Then, cells were fixed with 4% paraformaldehyde for 15 min in the dark and permeabilized with 0.2 % Triton X100 for 10 min at room temperature and washed again with PBS. Primary monoclonal antibody IgG against C_{60} (Santa Cruz Biotech Inc., Santa Cruz, USA) and polyclonal antibody against mouse IgG F7506 labeled with fluorescein isothiocyanate (FITC, Sigma-Aldrich Co., St-Louis, USA) were subsequently used according to (Grebinyk et al. 2018). Finally, the coverslips were rinsed with dH_2O, incubated with nucleus staining antifade solution (0.6 μM DAPI, 90 mM p-phenylenediamine in glycerol/PBS) for 2 h in the dark and sealed with slides.

Fluorescence microscopy was performed with the Keyence Microscope BZ-9000 BIOREVO (Osaka, Japan) equipped with blue (for DAPI, λ_{ex} = 377 nm, λ_{em} = 447 nm), green (for FITC, λ_{ex} = 472 nm, λ_{em} = 520 nm) and red (for MitoTracker, λ_{ex} 543 nm, λ_{em} = 593 nm) filters with the acquisition Software Keyence BZ-II Viewer (Osaka, Japan). The merged images and single-cell fluorescence intensity profiles were processed with the Keyence BZ-II Analyzer Software (Osaka, Japan).

Quantification of intracellular C_{60} accumulation

To study the accumulation dynamics we have extracted C_{60} from the cell homogenate as well as from the mitochondrial fraction and carried out high- performance liquid chromatography-electrospray ionization mass spectrometry (HPLC-ESI-MS, Shimadzu, Kyoto, Japan) analysis as previously established [36].

Briefly, HeLa cells (10^5/mL) were seeded in 6-well plates from Sarstedt, (Nümbrecht Germany). After 24 h cells were incubated for 0-48 h in the presence of 20 μM C_{60}. Cells were washed with PBS three times, harvested and frozen-thawed in distilled H_2O three times and dried at 80 °C under reduced pressure. C_{60} was extracted to toluene/2-isopropanol (6:1, v/v) via 1 h sonication. After centrifugation (70 min, 20 000 g) the toluene layer was analyzed with HPLC-ESI-MS. Chromatographic separation of C_{60} was performed using the column Eclipse XDV-C8 (Agilent, Santa Clara, USA) under isocratic elution conditions with a mobile phase of toluene and methanol. Optimized chromatographic conditions and MS parameters were recently published (Grebinyk et al. 2018).

The mitochondrial fraction, obtained according to [56], was used for extraction of C_{60} as described above, as well as for measurements of protein concentration [57] and succinate-reductase activity [58], used as a mitochondrial marker to testify enrichment and purity of the fraction.

Cell viability

HeLa cells (10^4/well), cultured in 96-well cell culture plates from Sarstedt (Nümbrecht, Germany) for 24 h, were treated with the 1 % FBS DMEM medium containing 20 μM C_{60} for 24 h and exposure to the 1 MHz US treatment. The control cells were treated without and with the equal volume of sterile water as a solvent of C_{60} colloid solution. Cell viability was determined with an MTT reduction assay [59] at 48 h after US treatment. Briefly, cells were incubated for 2 h at 37 °C in the presence of 0.5 mg/mL MTT. The diformazan crystals were dissolved in DMSO and determined at 570 nm with a microplate reader Tecan Infinite M200 Pro (Männedorf, Switzerland).

Cell viability assay was accompanied with the phase contrast microscopy analysis of HeLa cells under the study with the Keyence BZ-9000 BIOREVO (Osaka, Japan).

Caspase 3/7 Activity

HeLa cells were seeded into 96-well plates (10^4 cells/well) and incubated for 24 h. The cells were treated with 20 μM C_{60} for 24 h and subjected to US treatment (0, 20, 40, and 60 sec) as described above. Activity of caspases 3/7 was determined at 24 h after ultrasound exposure using the Promega Caspase-Glo® 3/7 Activity assay kit (Madison, USA) according to the manufacturer's instructions. Briefly, the plates were removed from the incubator and allowed to equilibrate to room temperature for 30 min. After treatment, an equal volume of Caspase-Glo 3/7 reagent containing luminogenic peptide substrate was added followed by gentle mixing with a plate shaker at 300 rpm for 1 min. The plate was then incubated at room temperature for 2 h. The luminescence intensity of the products of caspase 3/7 reaction was measured with the microplate reader Tecan Infinite M200 Pro (Männedorf, Switzerland).

Cell death type differentiation

HeLa cells, seeded in 6-well plates at a cell density of 6×10^4 cells/well in 1.5 mL of culture medium, were incubated for 24 h, then the medium was replaced with C_{60}-containing medium. After 24 h of incubation with C_{60} HeLa cells were treated with US as indicated above. At 24 h after US treatment cells were harvested. Apoptosis was detected by Annexin V-fluorescein isothiocyanate/propidium iodide apoptosis detection kit according to the manufacturer's instructions. Briefly, cells were harvested and washed with binding buffer. After the addition of FITC-conjugated Annexin V cells were incubated for 15 min at room temperature in dark. Cells were washed with Binding buffer and at 10 min after propidium iodide addition were analyzed with the BD FACSJazz™ (BD Biosciences, Singapore). A minimum of 2×10^4 cells per sample were acquired and analyzed with the BD FACS™ Software (BD Biosciences, Singapore).

On every histogram of flow cytometry four populations of cells are presented according to green (Annexin V-FITC) and red propidium iodide (PI) fluorescence intensities: viable (Annexin V-FITC negative, PI negative), early apoptotic (Annexin V-FITC positive, PI negative), late apoptotic (Annexin V-FITC positive, PI positive) and necrotic (Annexin V-FITC negative, PI positive) cells.

Statistics

All experiments were carried out with a minimum of four replicates. Data analysis was performed with the use of the GraphPad Prism 7 (GraphPad Software Inc., San Diego, California, USA). Paired Student's t-tests were performed. The significance level was set at $p < 0.01$.

Declarations

Acknowledgements

We thank the German Academic Exchange Service (DAAD) for their support (scholarship for AG 57129429 and AR 91775672) and the Brandenburg programme “Strengthening technological and application-oriented research at scientific institutions (StaF Directive)” (FullDrug, 85037298). We also thank for the support of the Open Access Publication Funds by the German Research Foundation and of the Technical University of Applied Sciences Wildau.

We express our deep gratitude to Michael Danese from Kaijo Shibuya America Inc. (Santa Clara CA, USA) for the generous gift of both ultrasound transducer and generator as well as to Yumiko Iwasaki for organization of its shipment.

We thank ViNN:Lab (Technical University of Applied Sciences Wildau, Germany) for 3D printing of the plate holder.

Author contributions

The presented work was carried out in collaboration between all authors. M.F. coordinated the research and provided resources. J.G. proposed the original idea and assisted the experimental work. S.P. and U.R. synthesized C_{60}. S.G. carried out mass spectrometry. A.G. performed DLS. A.R. performed sonoluminescence intensity measurements. A.R., B.K. and A.G. performed cell-based assays, prepared figures, and performed the statistical analysis. A.R., A.G., O.Z. and M.F. analysed the data and wrote the manuscript. All authors discussed the results and commented on the manuscript.

Competing Interests

The authors declare that they have no competing interests.

Data availability

The datasets used and analysed during the current study are available from the corresponding author on reasonable request.

References

1. Kroto, H., Heath, J., O’Brien, S., Curl, R., Smalley, R. C_{60}: Buckminsterfullerene. Nature **318**, 162–163 (1985).
2. Anilkumar, P. *et al*. Fullerenes for Applications in Biology and Medicine. Current Medicinal Chemistry **18**, 2045–2059 (2011).
3. Haddon, R. Electronic structure, conductivity and superconductivity of alkali metal doped (C_{60}). Acc Chem Res American Chemical Society **25**, 127–133 (1992).
4. Hamblin, M. Fullerenes as Photosensitizers in Photodynamic Therapy: Pros and Cons. Photochem Photobiol Sci. **17**, 1515–1533 (2018).

5. Sharma, S., Chiang, L., Hamblin, M. Photodynamic therapy with fullerenes in vivo: reality or a dream? Nanomedicine (Lond) **6**, 1813–1825 (2011).
6. Orlova, M. Perspectives of Fullerene Derivatives in PDT and Radiotherapy of Cancers. British Journal of Medicine and Medical Research **3**, 1731–1756 (2013).
7. Ritter, U. *et al.* Structural Features of Highly Stable Reproducible C_{60} Fullerene Aqueous Colloid Solution Probed by Various Techniques. Fullerenes, Nanotubes and Carbon Nanostructures **23**, 530–534 (2015).
8. Prylutska, S. *et al.* Study of C_{60} fullerenes and C_{60}-containing composites cytotoxicity in vitro. Materials Science and Engineering: C **27**, 1121–1124 (2007).
9. Prylutska, S. *et al.* Comparative study of biological action of fullerenes C_{60} and carbon nanotubes in thymus cells. Materialwissenschaft und Werkstofftechnik **40**, 238–241 (2009).
10. Grebinyk, A. *et al.* C_{60} fullerene accumulation in human leukemic cells and perspectives of LED-mediated photodynamic therapy. Free Radic Biol Med. **124**, 319–327 (2018).
11. Palyvoda, K., Grynyuk, I., Prylutska, S., Samoylenko, A., Drobot, L., Matyshevska, O. Apoptosis photoinduction by C_{60} fullerene in human leukemic T cells. Ukr. Biokhim. Zh. **82**, 121–127 (2010).
12. Scharff, P. *et al.* Therapeutic reactive oxygen generation. Tumori **94**, 278–283 (2008).
13. Pac, B., Petelenz, P., Eilmes, A., Munn, R. Charge-transfer exciton band structure in the fullerene crystal-model calculations. J. Chem. Phys. **109**, 7923–7931 (1998).
14. Ash, C., Dubec, M., Donne, K., Bashford, T. Effect of wavelength and beam width on penetration in light-tissue interaction using computational methods. Lasers Med. Sci. **32**, 1909–1918 (2017).
15. Zhang, H. *et al.* Penetration depth of photons in biological tissues from hyperspectral imaging in shortwave infrared in transmission and reflection geometries. J. Biomed. Opt. **21**, 126006 (2016).
16. Costley, D. *et al.* Treating cancer with sonodynamic therapy: A review. International Journal of Hyperthermia **31**, 107–117 (2015).
17. Putterman, S., Weninger, K. Sonoluminescence: How Bubbles Turn Sound into Light. Annual Review of Fluid Mechanics **32**, 445–476 (2000).
18. Didenko, Y., Pugach, S. Spectra of Water Sonoluminescence. The Journal of Physical Chemistry **98**, 9742–9749 (1994).
19. Gaitan, D. *et al.* Spectra of single-bubble sonoluminescence in water and glycerin-water mixtures. Physical Review E. **54**, 525–528 (1996).
20. Zolfagharpour, F., Khalilabad, M., Nikkhoo, N., Mousavi, M., Hatampanah, S. Spectrum of emitted light from sonoluminescence bubbles. Advances in Applied Physics **1**, 93–103 (2013).
21. Canteenwala, T., Padmawar, P., Chiang, L. Intense Near-Infrared Optical Absorbing Emerald Green [60]Fullerenes. J Am Chem. Soc. **127**, 26–27 (2005).
22. Li, Y. *et al.* 5-Aminolevulinic Acid-Based Sonodynamic Therapy Induces the Apoptosis of Osteosarcoma in Mice. PLOS ONE Public Library of Science **10**, e0132074; 10.1371/journal.pone.0132074 (2015).

23. Ohmura, T. *et al.* Sonodynamic Therapy with 5-Aminolevulinic Acid and Focused Ultrasound for Deep-seated Intracranial Glioma in Rat. Anticancer Research **31**, 2527-2533 (2011).
24. Chen, Y. *et al.* A theranostic nrGO@MSN-lON nanocarrier developed to enhance the combination effect of sonodynamic therapy and ultrasound hyperthermia for treating tumor. Nanoscale **8**, 12648–12657 (2016).
25. Li, E. *et al.* Sinoporphyrin sodium based sonodynamic therapy induces anti-tumor effects in hepatocellular carcinoma and activates p53/caspase 3 axis. Int J Biochem Cell Biol. **113**, 104-114 (2019).
26. Gao, F. *et al.* Titania-coated 2D gold nanoplates as nanoagents for synergistic photothermal/sonodynamic therapy in the second near-infrared window. Nanoscale **11**, 2374–2384 (2019).
27. Wang, J., Jiao, Y., Shao, Y. Mesoporous Silica Nanoparticles for Dual-Mode Chemo-Sonodynamic Therapy by Low-Energy Ultrasound. Materials **11**, 2041 (2018).
28. You, D. *et al.* ROS-generating TiO_2 nanoparticles for non-invasive sonodynamic therapy of cancer. Scientific Reports Nature Publishing Group **6**, 23200 (2016).
29. Tabata, Y. *et al.* Sonodynamic Effect of Polyethylene glycol-conjugated Fullerene on Tumor. In: Ōsawa E, (ed. Perspectives of Fullerene Nanotechnology Dordrecht: Springer Netherlands) 185-196 (2002).
30. Yumita, N., Watanabe, T., Chen, F., Momose, Y., Umemura, S. Induction of Apoptosis by Functionalized Fullerene-based Sonodynamic Therapy in HL-60 cells. Anticancer Research International Institute of Anticancer Research **36**, 2665–2674 (2016).
31. Iwase, Y. *et al.* Antitumor effect of sonodynamically activated pyrrolidine tris-acid fullerene. Japanese Journal of Applied Physics **55**, 07KF02; 10.7567/JJAP.55.07KF02 (2016).
32. Qiao, R., Roberts, A., Mount, A., Klaine, S., Ke, P. Translocation of C_{60} and Its Derivatives Across a Lipid Bilayer. Nano Lett. **7**, 614–619 (2007).
33. Santos, S. *et al.* Interaction of fullerene nanoparticles with biomembranes: from the partition in lipid membranes to effects on mitochondrial bioenergetics. Toxicol. Sci. **138**, 117–129 (2014).
34. Wagner, T., Magill, C., Herrle, J. Carbon Isotopes. In: White WM, (ed. Encyclopedia of Geochemistry: A Comprehensive Reference Source on the Chemistry of the Earth Cham: Springer International Publishing) 194–204 (2018).
35. Prylutskyy, Y. *et al.* C_{60} fullerene aggregation in aqueous solution. Phys. Chem. Phys. **15**, 9351–9360 (2013).
36. Grebinyk, A. *et al.* HPLC-ESI-MS method for C_{60} fullerene mitochondrial content quantification. Data Brief. **19**, 2047–2052 (2018).
37. Mroz, P. *et al.* Intraperitoneal photodynamic therapy mediated by a fullerene in a mouse model of abdominal dissemination of colon adenocarcinoma. Nanomedicine **7**, 965–974 (2011).

38. Lee, D., Ahn, Y., Youn, Y., Lee, E. Poly(ethylene glycol)-crosslinked fullerenes for high efficient phototherapy: multimeric fullerenes. Polymers for Advanced Technologies **24**, 220–227 (2013).
39. Li, Z. *et al.* 5-Aminolevulinic acid-loaded fullerene nanoparticles for in vitro and in vivo photodynamic therapy. Photochem Photobiol. **90**, 1144–1149 (2014).
40. Brenner, M., Hilgenfeldt, S., Lochse, D. Single-bubble sonoluminescence. Reviews of modern physics **74**, 425-484 (2002).
41. Scharff, P., Risch, K., Carta-Abelmann, L. et al., Structure of C60 fullerene in water: Spectroscopic data. Carbon **42**, 1203-1206 (2004).
42. Rossi, G., Barnoud, J., Monticelli, L. Partitioning and solubility of C_{60} fullerene in lipid membranes. Phys. Scr. **87**, 058503; 10.1088/0031-8949/87/05/058503 (2013).
43. Levi, N., Hantgan, R., Lively, M., Carroll, D., Prasad, G. C_{60}-Fullerenes: detection of intracellular photoluminescence and lack of cytotoxic effects. J Nanobiotechnology **4**, 14 (2006).
44. Braden, B. *et al.* X-ray crystal structure of an anti-Buckminsterfullerene antibody Fab fragment: Biomolecular recognition of C_{60}. Proceedings of the National Academy of Sciences **97**, 12193–12197 (2000).
45. Chen, B., Wilson, S., Das, M., Coughlin, D., Erlanger, B. Antigenicity of fullerenes: Antibodies specific for fullerenes and their characteristics. Proceedings of the National Academy of Sciences **95**, 10809–10813 (1998).
46. van Wezel, A., Morinière, V., Emke, E., ter Laak, T., Hogenboom, A. Quantifying summed fullerene nC_{60} and related transformation products in water using LC LTQ Orbitrap MS and application to environmental samples. Environ. Int. **37**, 1063–1067 (2011).
47. Chistyakov, V., Prazdnova, E., Soldatov, A., Smirnova, Y., Alperovich, I. Can C_{60} fullerene demonstrate properties of mitochondria-targeted antioxidant from the computational point of view? International Journal of Biology and Biomedical Engineering **8**, 59-62 (2014).
48. Emelyantsev, S., Prazdnova, E., Chistyakov, V., Alperovich, I. Biological Effects of C_{60} Fullerene Revealed with Bacterial Biosensor—Toxic or Rather Antioxidant? Biosensors **9**, 81 (2019).
49. Chirico, F. *et al.* Carboxyfullerenes localize within mitochondria and prevent the UVB-induced intrinsic apoptotic pathway. Exp. Dermatol. **16**, 429–436 (2007).
50. Zhou, F., Wu, S., Yuan, Y., Chen, W., Xing, D. Mitochondria-targeting photoacoustic therapy using single-walled carbon nanotubes. Small **8**, 1543–1550 (2012).
51. Hensel, K., Mienkina, M., Schmitz, G. Analysis of ultrasound fields in cell culture wells for in vitro ultrasound therapy experiments. Ultrasound Med. Biol. **37**, 2105–2115 (2011).
52. Secomski, W. *et al.* In vitro ultrasound experiments: Standing wave and multiple reflections influence on the outcome. Ultrasonics **77**, 203–213 (2017).
53. Merritt, C. Ultrasound safety: what are the issues? Radiology Radiological Society of North America **173**, 304–306 (1989).

54. World Health Organization. Environmental Health Criteria 22. Ultrasound. Published under the joint sponsorship of the United Nations Environment Programme, the World Health Organization and the International Radiation Protection Association https://stg-wedocs.unep.org/bitstream/handle/20.500.11822/29309/EHC22Ultrsnd.pdf?sequence=1&isAllowed=y (1982).
55. Liyan, L., Yang, Y., Penghong, L., Wei, T. The influence of air content in water on ultrasonic cavitation field. Ultrasonics Sonochemistry **21**, 566-571 (2014).
56. Frezza, C., Cipolat, S., Scorrano, L. Organelle isolation: functional mitochondria from mouse liver, muscle and cultured filroblasts. Nature Protocols **2**, 287–295 (2007).
57. Bradford, M. A rapid and sensitive method for the quantitation of microgram quantities of protein utilizing the principle of protein-dye binding. Anal Biochem. **72**, 248–254 (1976).
58. Pennington, R. Biochemistry of dystrophic muscle. Mitochondrial succinate–tetrazolium reductase and adenosine triphosphatase. Biochem. J. **80**, 649–654 (1961).
59. Carmichael, J., DeGraff, W., Gazdar, A., Minna, J., Mitchell, J. Evaluation of a tetrazolium-based semiautomated colorimetric assay: assessment of chemosensitivity testing. Cancer Res. **47**, 936–942 (1987).

Figures

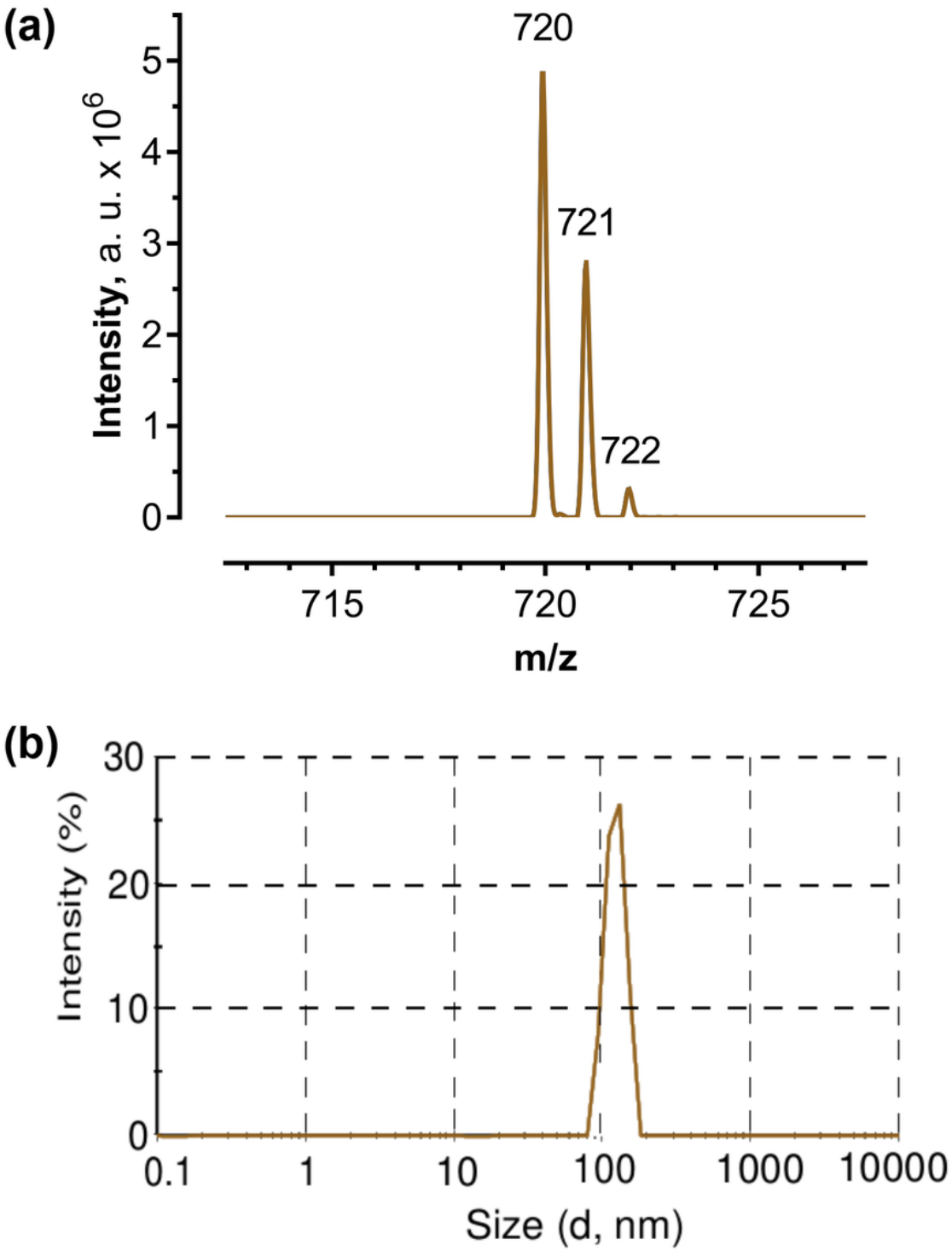

Figure 1

C_{60} aqueous colloid solution: **(a)** – MALDI-TOF-MS spectrum of C_{60} colloid solution, a.u. = arbitrary units; **(b)** – Hydrodynamic size (diameter, nm) of 20 μM C_{60}, Intensity (%): percentage of all scattered light intensity.

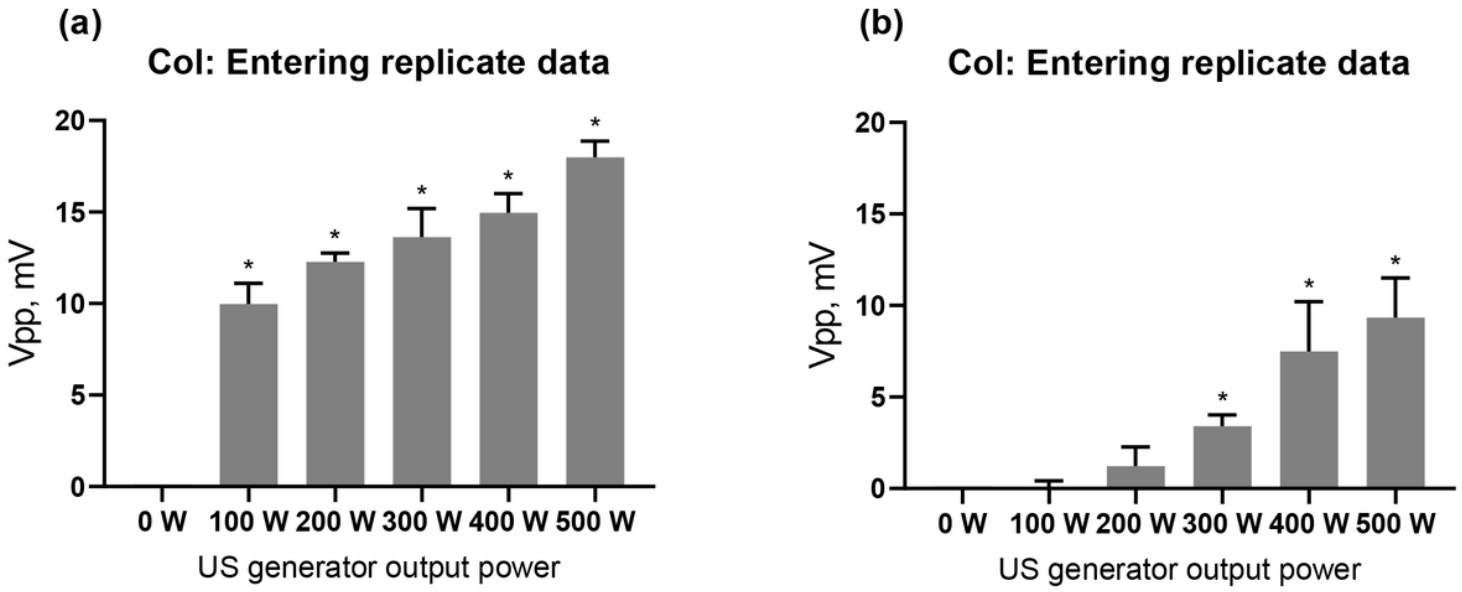

Figure 2

Sonoluminescence intensity: **(a)** – in the US bath, **(b)** – in well of the plate.

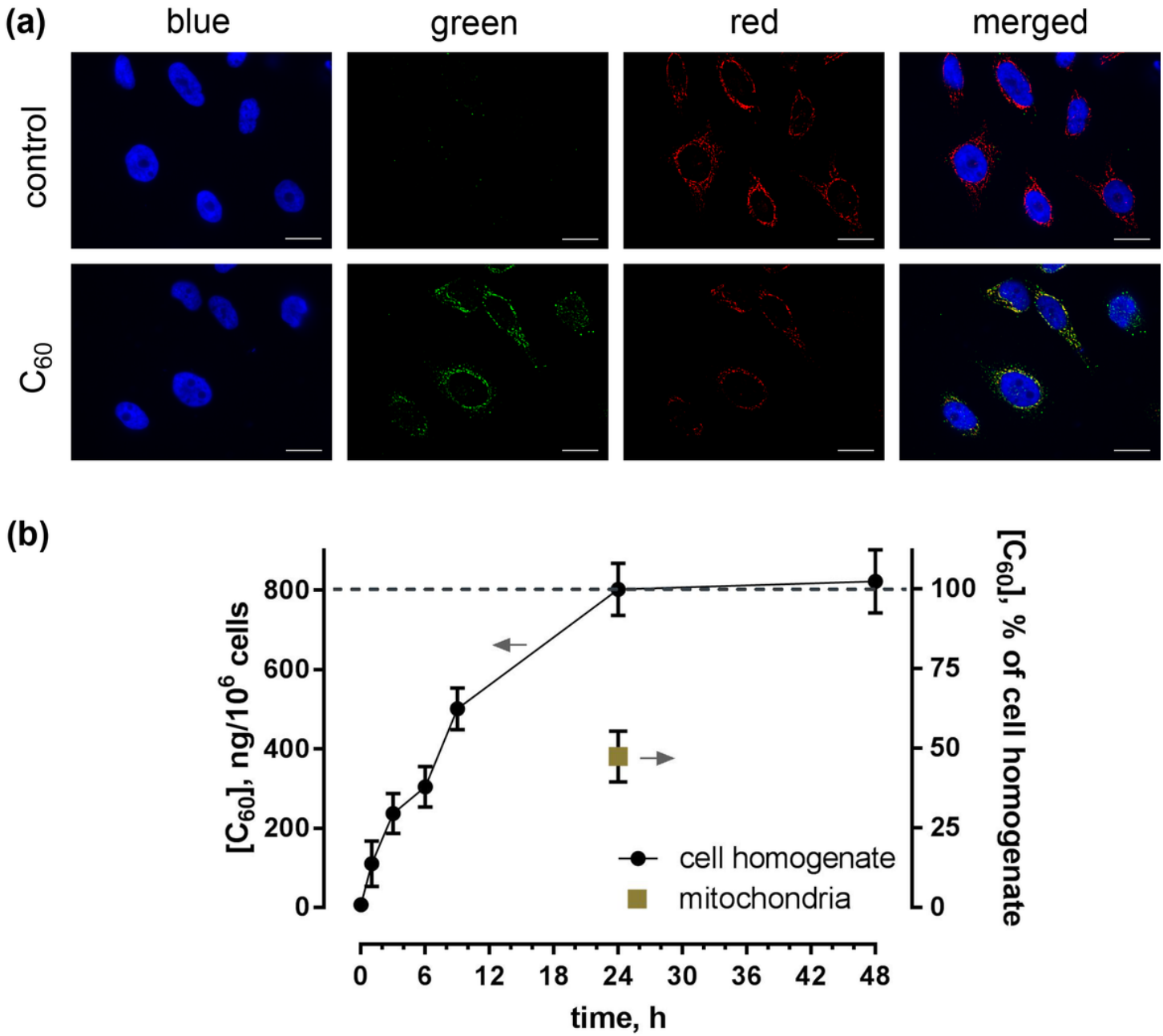

Figure 3

Uptake of C_{60} in HeLa cells: **(a)** – Fluorescence microscopy images of HeLa cells, incubated for 24 h with 20 μM C_{60} and stained with DAPI (blue), MitoTrecker (red) and FITC-labeled antibody against C_{60} (green), scale bar 20 μm; **(b)** – HPLC-ESI-MS analysis of C_{60} content in toluene extracts from cell homogenate and mitochondrial fraction after incubation of cells in the presence of 20 μM C_{60}.

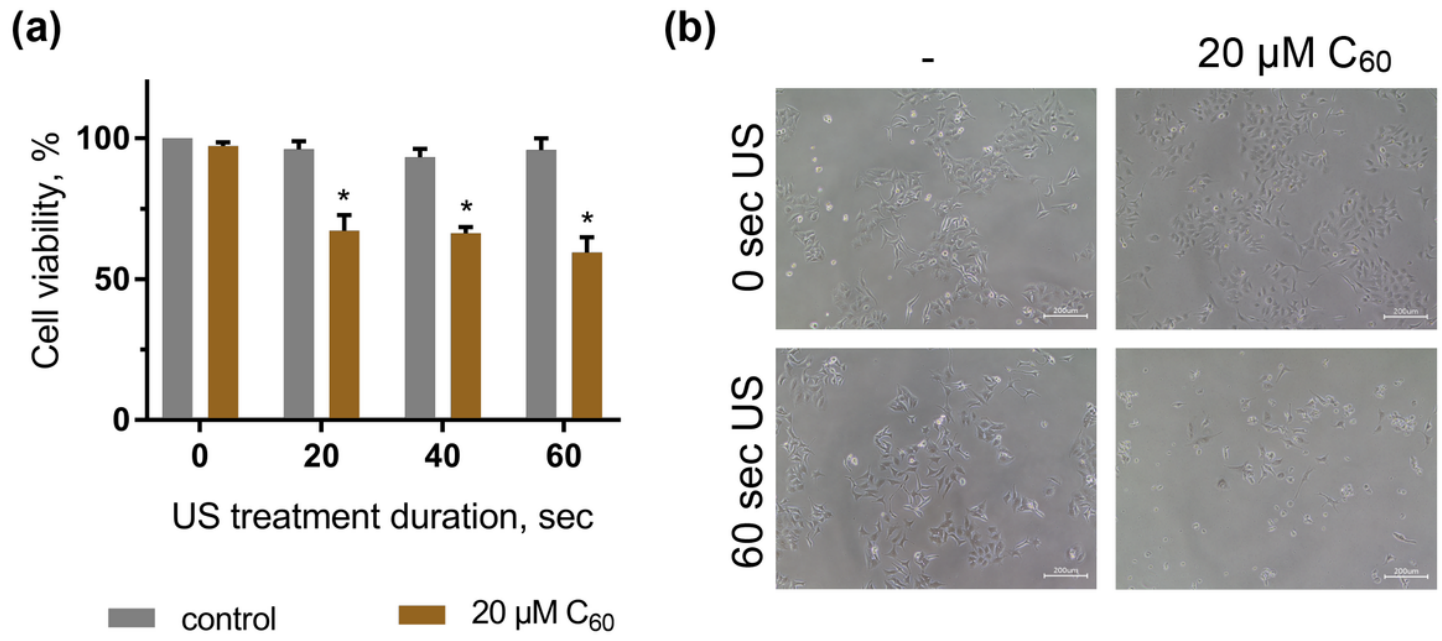

Figure 4

Viability of HeLa cells, incubated in the presence of 20 μM C_{60} and treated with 1 MHz ultrasound (US): **(a)** – MTT assay, * – $p \leq 0.01$ in comparison with viability of cells, treated with respective duration of US; **(b)** – Phase contrast microscopy images of HeLa cells, incubated in the presence of 20 μM C_{60} and treated with 60 sec ultrasound, scale bar 200 μm.

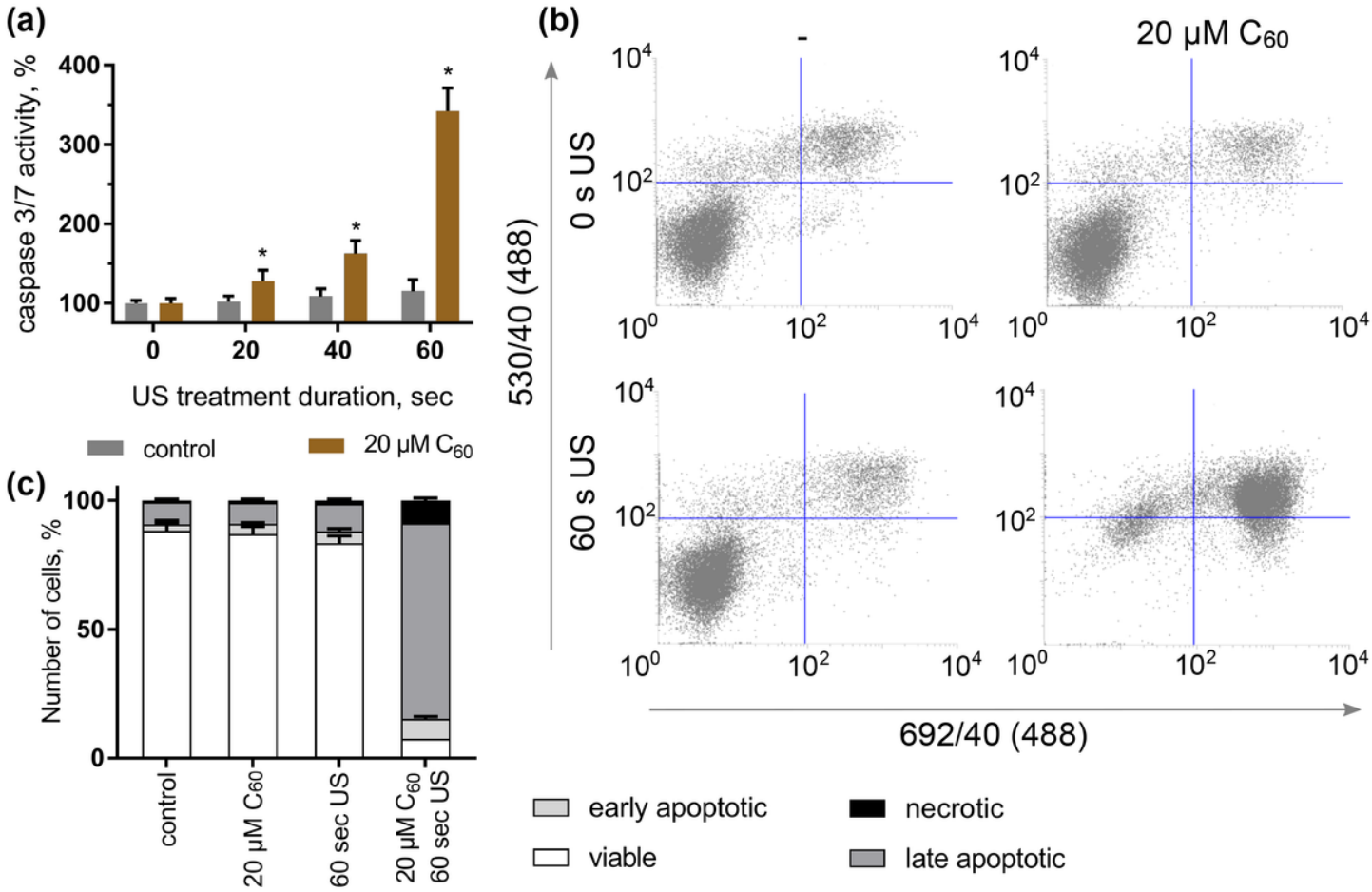

Figure 5

Apoptosis induction in HeLa cells by sonodynamically excited C_{60}: **(a)** – Caspase 3/7 activity, * – $p \leq 0.01$ in comparison with viability of cells, treated with respective duration of US; **(b)** – FACS histograms of HeLa cells, stained with Annexin V-FITC/PI (in each panel the lower left quadrant shows the content of viable, upper left quadrant – early apoptotic, upper right quadrant – late apoptotic, lower right quadrant – necrotic cells populations); **(c)** – Quantitative analysis of cell population content, differentiated with double Annexin V-FITC/PI staining.

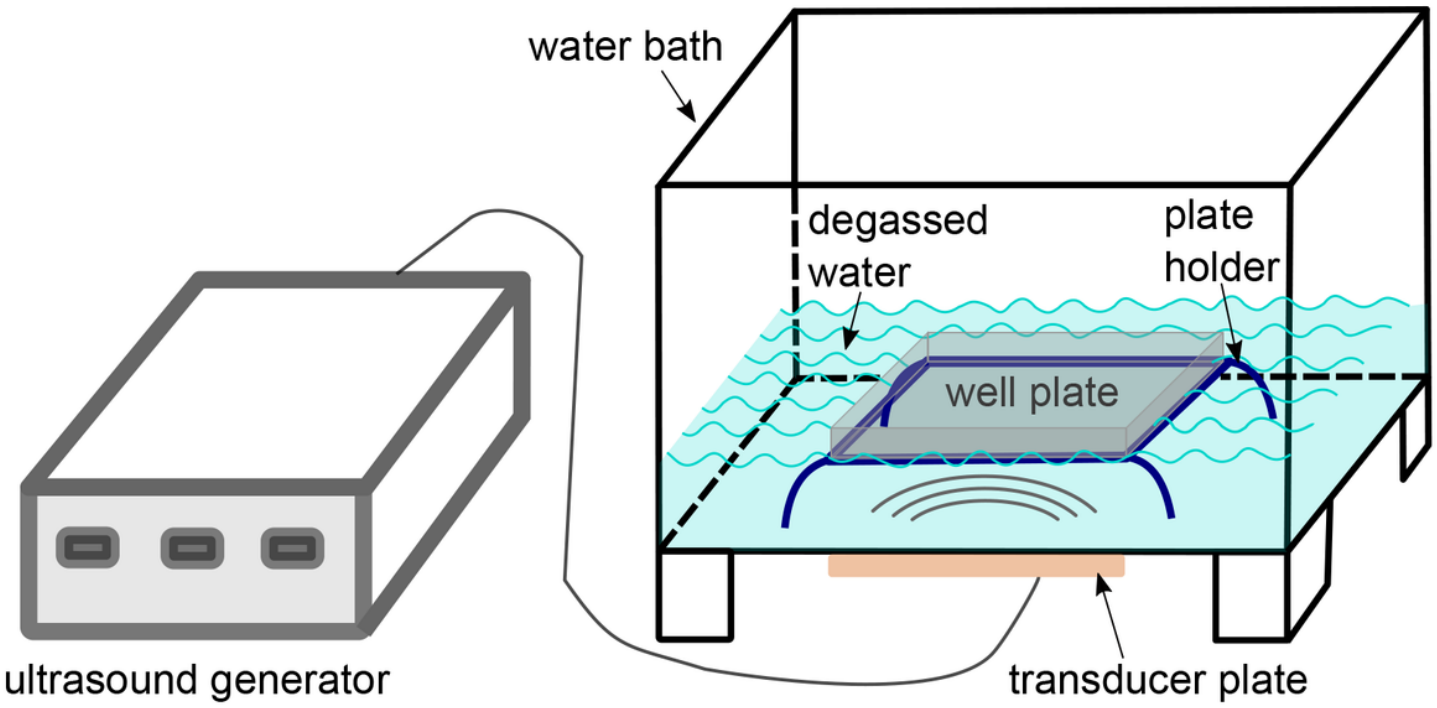

Figure 6

Diagram of the ultrasound exposure equipment.